



An eco-friendly corrosion inhibitor *Cuscuta reflexa* extract and PEG400 for mild steel inhibition in acidic medium: computational and experimental investigations

Priti Pahuja¹ · Meena Yadav¹ · Monika Dhanda¹ · Rajat Arora¹ · Simran Ahlawat¹ · Ajay Satija² · Neeru Jhanjhariya¹ · Sumit Kumar¹ · Suman Lata¹ 

Received: 30 June 2022 / Accepted: 22 October 2022 / Published online: 5 November 2022
© The Author(s), under exclusive licence to Springer-Verlag GmbH Germany, part of Springer Nature 2022

Abstract

Herein, the mechanism of corrosion prevention of mild steel (MS) by extract of *Cuscuta reflexa* Amarbel (AME) as green inhibitor is explained by gravitational, electrochemical measurements. The viability of neat extract and after adding an intensifier was investigated as corrosion inhibitor for MS in hydrochloric acid. The presence of electron-rich moieties in AME was characterized through Fourier-transform infrared spectroscopy (FTIR). Furthermore, polarization measurements showed that AME acted as a mixed type inhibitor against corrosion. The formulation of 100 ppm AME with 50 ppm polyethylene glycol 400 (PEG400) as an intensifier showed inhibition efficiency of 97.51% for MS in 0.5 M HCl. The protection of MS in (AME + PEG) formulation was also assessed through the Langmuir, Freundlich, and Flory–Huggins adsorption isotherm model. The surface studies of the MS were examined by atomic force microscopy (AFM) and scanning electron microscopy (SEM) that indicated a smoothed surface of the metal in the presence of the studied compounds. XPS study was executed to analyze the interaction of the inhibitor with the metal surface. In addition, computational quantum study provides the molecular structural relationship with corrosion inhibitive competence of the extract.

Keywords Mild steel · Plant extract · Corrosion inhibition · AFM and XPS

Introduction

Owing primarily to its utility in infrastructure and industries, carbon steel/mild steel is one of the most widely used steel alloys. However, low corrosion resistance in its working atmosphere specifically in acidic medium is the challenging factor to deal with. Corrosion is an electrochemical process that occurs due to the highly reactive nature of metal. The numerous aspects like composition, presence of oxygen/moisture, strong acid or base, impurities, corrosive aerosols, and bacteria subsequently leads to deterioration of the

metal. All these electrochemical factors are responsible for the initiation of corrosive electrochemical reactions (Fazal et al. 2022; Naderi et al. 2022; Olusegun et al. 2016). The corrosive products create a threat to the environment, and in turn, damage may be faced by every sector like residential, commercial, institutional, and industrial (Qiang et al. 2018; Kumar et al. 2017a, b; Afia et al. 2015).

The impact of corrosion can be minimized by applying suitable anticorrosive techniques, out of which the use of corrosion inhibitors (Arukalam et al. 2020; Dariva and Galio n.d.; Sambyal et al. 2018) is proven as one of the most preferred solutions for effective protection of metals (Yao et al. 2020). Corrosion inhibitors are the chemical substances that are being added in very low dosage during acid pickling in industries and are helpful in minimizing the corrosion either by passivation or by maintaining the pH by acting as a buffer (Saini et al. 2019). Over the past decade, organic and inorganic moieties as corrosion inhibitors have been frequently used; however, the serious issues arise due to the toxicity of commercially available organic and inorganic type inhibitors. Recently, green corrosion inhibitors (Rani and Basu 2012) are the main concern

Responsible Editor: Philippe Garrigues

✉ Suman Lata
sumanjakhar.chem@dcrustm.org

¹ Department of Chemistry, Deenbandhu Chhotu Ram University of Science and Technology, Murthal 131039, Haryana, India

² Department of Applied Science and Humanities, Inderprastha Engineering College, Ghaziabad, India

in lieu of increasing environmental noxiousness, and for that purpose, various new plant materials as green inhibitors need to be explored to enhance, recycle, and reuse characteristic potent ability of such environmental friendly resources. Plant extracts (Abdullah Dar 2011) are of great practical significance with ample availability, environmental sustainability and profitable cost which are also capable of producing intended results (Kesavan et al. 2012).

The former scrutiny reveals that plant extracts (Raja and Sethuraman 2008) are well accomplished with flavonoids, alkaloids and polyphenols and possess many such electron-rich moieties (Shehata et al. 2018; Raja et al. 2013). Several plant extracts have been tested as corrosion inhibitors in an acidic medium for low alloy steel/MS: *Aloe vera* leaf extract (Mehdipour et al. 2015), *Acalypha torta* leaves (Krishnegowda et al. 2013), *Justicia gendarussa* (Satapathy et al. 2009) and *Sida acuta* (Umoren et al. 2016). Herein, a parasitic plant found all over India with a common name as Amarbel and with the scientific name as *Cuscuta reflexa* is explored as a corrosion controlling candidate. Though this parasitic stem is being used for medicinal purposes (Ahmad et al. 2017; Vijikumar et al. 2011), unfortunately, its exponential growth (once initiated) over other medicinal trees and plants, curbing their nurturing and natural aging, indicates its harmful effects, which also diminishes the beneficial activity of these plants. In the present study, Amarbel alone and Amarbel with intensifier polyethylene glycol 400 (PEG400) have been examined as corrosion controlling agents for mild steel in the hydrochloric acid medium. The novelty of the work evidences about the fact that no reports regarding performance of AME + PEG400 as a green inhibitor in 0.5 M HCl are found till date. PEG400 is a hydrophilic polymer with an environmentally friendly nature. The importance of PEG as corrosion inhibitor agent is related with its capability to get adsorbed over the surface of the metal and thus blocking the active sites of metal (Boudehlioua et al. 2019; Deyab 2018; Fares et al. 2013). First, the study is focussed to investigate the optimized concentration of this combination in order to work as best formulation to control metal dissolution in 0.5 M HCl. Thereafter, the inhibition capabilities have been studied using weight loss, electrochemical techniques (potentiodynamic polarization, electrochemical impedance spectroscopy) and simulation computational methods. Subsequently, the mechanism of interaction between AME and MS is proposed.

Experimental strategy

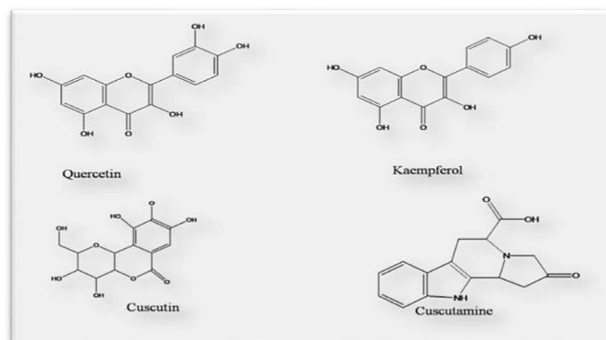
Materials and methods

Amarbel strings like parasitic inter-twined stem were accumulated from host trees located around IIT, Delhi, India.

Hydrochloric acid with 35.4% purity, ethanol, PEG-400 and all other reagents used were collected from Sigma Aldrich. The preparation of test solution from 100 to 800 ppm concentration from Ame extract varied by addition of 0.5 M HCl.

Synthesis of plant extract and inhibitory solutions

The shed dried Amarbel parasitic stem was first washed with double-distilled water to remove dust and then dried at 40 °C in an oven for 4 h to remove moisture. Five grams of powdered leaves was refluxed in 100 mL ethanol for 5 h at 80 °C. The extract obtained was filtered and dried to evaporate the solvent (Pahuja et al. 2020). This ethanolic Amarbel extract (AME) obtained in powdered form was used for the preparation of inhibitory solutions of required concentration (100–800 ppm) through dissolving in 0.5 M HCl medium. The best formulation of Ame with PEG was prepared in 2:1 ratio; herein, 100 mg L⁻¹ Ame and 40 mg L⁻¹ polyethylene glycol 400 (PEG400) inhibitor solution was prepared in 0.5 M HCl. The major electron-rich constituents of AME, i.e. quercetin (I), cuscutin (II), kaempferol (III) and cuscutamine (IV) possess the structures as below (Ahmad et al. 2017; Vijikumar et al. 2011).



Preparation of specimens and corrosion tests

Weight loss measurements

The corrosion inhibitive effect of AME was evaluated for MS steel specimens with the chemical composition (w/w %) as C = 0.14, Si = 0.05, Mn = 0.032, S = 0.05, P = 0.02, Ni = 0.01, Cu = 0.01 Cr = 0.01 and balance as Fe. The specimens were consequently abraded and polished with different grade of emery papers ranging from 320 to 2000 for maximum smoothness. Before the usage of these specimens for weight loss measurements, they were degreased with acetone, washed with

water, then dried and weighed possessing dimensions as 2.5 cm × 2.5 cm × 0.028 cm. The weight loss experiments were performed in thermostat to maintain the experimental temperature. All the weight loss investigations were performed repeatedly with the standard error found within ± 0.01 limits.

Electrochemical experiments

Electrochemical measurements were performed by exploiting PGSTAT204, Autolab, Netherland with FRA32M module installed with NOVA 1.11 software. The measurements were conducted with three-electrode assembly with silver/silver chloride as reference electrode, graphite electrode as a counter electrode and MS specimens with area 1 cm² acted as the working electrode. To minimize the chances of IR drop, luggin probe tip was made in close proximity to the working electrode. Each time, the electrochemical cell was maintained for 30–35 min, in the respective corrosive medium to attain the open circuit potential. The open circuit potential (OCP) vs. time curve is shown in Fig. S1a in Supplementary section S1.1. The OCP of the MS working electrode in the presence of AME extract reached a stable level after 1600 s of immersion. OCP values are given at AME concentrations of 0 ppm, 100 ppm, 200 ppm, 400 ppm, 600 ppm and 800 ppm. A general tendency to shift the OCP to a more positive side emerges, indicating assimilation of the inhibitor species across the metal surface. Thereafter, potentiodynamic polarization (PP) was evaluated with a scan rate of 0.001 V/s in potential range from –250 to +250 mV. Electrochemical impedance spectroscopy (EIS) measurement was performed from 100 kHz to 0.1 Hz through ac signal of 5 mV amplitude. EIS gives values of charge transfer resistance (R_{CT}) and maximum frequency (f_{max}) (Kumar et al. 2017a, b). The experimental measurements were commenced at 303 K, 313 K and 323 K.

Surface characterization

The presence of electron-rich moieties in AME was characterized by a Fourier transform infrared spectrometer Perkin-Elmer model FT-IR/RZX. The morphological variation of the corroded metal surface of each MS specimen with size 1 cm² was evaluated in standard mode with Atomic Force Microscopy (AFM) Instrument (Model: Nanosurf Nao) from Molecular Image (Pico Scan). Micro-fabricated single-beam Si₃N₄ has resonance frequency in the range of 13 kHz. All the scanning electron microscopy (SEM) images were taken at ×3000 magnification with Model Zeiss Ultra 55 at 3 kV for SEM technique. X-ray photoelectron spectroscopy (XPS) analysis was performed using a PHI 5000 versaprobe III.

Theoretical observations and depiction

The quantum-related observables were envisaged for the AME using density functional theory (DFT) (El Aoufir et al. 2017). The parameters born via quantum approach were accomplished using Gaussian 09. The quantum chemical descriptors such as E_{HOMO} , E_{LUMO} , ΔE got via ($E_{LUMO} - E_{HOMO}$) and ΔN (number of fractional electrons), electronegativity (χ) and absolute hardness (η), almost all were taken into consideration (Titi et al. 2018). The quantum tools were studied in order to correlate and depict the various envisaged observables with the experimental findings.

The molecular dynamics (MD) simulations were done utilizing Forcite module of Material Studio. In this case, the iron crystal was imported from Material Studio information base and severed along (1 1 0) plane, and a slab of 6 Å was utilized. The decision of selecting Fe (1 1 0) as a substrate was related on the fact that it is found to have high stabilization energy and an exceptionally packed structure. The Fe (1 1 0) surface was loose and afterwards augmented to a 10 × 10 supercell to give an enormous surface to support the association of the inhibitor with iron surface. A vacuum slab with zero thickness was assembled. A simulation box with a size of 24.76 × 24.76 × 45.00 Å³ containing two layers was made utilizing the layer builder module of the Material Studio so as to make the recreation closer to the real system. The first layer at the base contained iron atoms and one layer above contained 500 H₂O, 9H⁺, 9Cl⁻ and 1 molecule of inhibitor. All simulations were operated utilizing COMPASSII power field, a period step of 1 fs, a simulation session of 2000 ps and the canonical NVT at 303 K.

Results and discussion

FTIR analysis

The interpretation of Fourier transform infrared spectroscopy (FTIR) peaks (Fig. 1) ranges from 4000 to 400 cm⁻¹ and shows that the AME contain phenolic, carboxylic, methyl, ketonic and amide groups. The main peaks have been observed in the FTIR spectrum: 3947 cm⁻¹, 3409 cm⁻¹, 2846 cm⁻¹, 1851 cm⁻¹, 1735 cm⁻¹, 1380 cm⁻¹, 1058 cm⁻¹. The peaks 3947 cm⁻¹ and 3830 cm⁻¹ are assigned to NH (imine) and NH₂ (amine). The band 1058 cm⁻¹ corresponds to –C–O–C. The peak at 3409 cm⁻¹ indicates the presence of the phenolic group. The bands 750–450 cm⁻¹ appearing in this range may be contributed by symmetrical and asymmetrical bending vibration of COC (Satapathy et al. 2009; Chevalier et al. 2014).

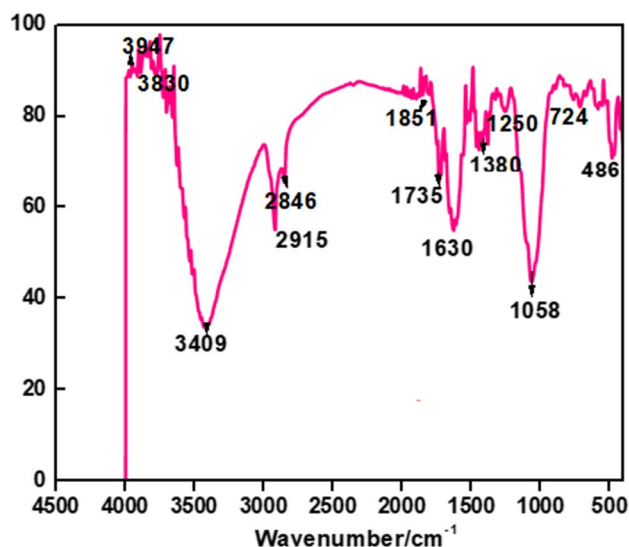


Fig. 1 FTIR of Amarbel extract (AME)

Weight loss measurements

The MS specimens were immersed in 0.5 M HCl for 4 h in the absence and presence of AME alone and AME with intensifier (PEG400). The corrosion rate was evaluated by the use of Eq. 1:

$$\text{Corrosion rate (CR)} = \frac{87.6 \times \Delta w}{\text{DAT}} \quad (1)$$

where Δw is actual weight loss (mg), D is MS density (7.86 g cm^{-3}), A is the total area (cm^2) affected by corrosion, and T is the immersion time in h. The CR values were used to calculate the inhibition efficiency (η) by the following equation:

$$\eta \% = \frac{CR^0 - CR}{CR^0} \times 100 \quad (2)$$

Here, CR and CR^0 are the values of the rate of corrosion of MS with and without inhibitors.

The η of AME at 100 ppm was 86.35% as shown in Table 1 that was maximized as 96.34% at 800 ppm.

Table 1 Corrosion rate (CR) and % inhibition efficiency (η) of AME obtained from weight loss measurement in 0.5 M HCl

Corrosive medium	Concentration (ppm)	CR (mmpy) at 303 K	η %	CR (mmpy) at 313 K	η %	CR (mmpy) at 323 K	η %
0.5 M HCl	Blank	24.98	–	44.60	–	73.15	–
	100	3.41	86.35	13.00	70.86	27.08	62.98
	200	2.47	90.10	5.48	87.71	10.26	85.98
	400	1.45	94.20	3.66	91.80	7.96	89.12
	600	1.25	94.99	2.36	94.70	3.92	94.64
	800	0.83	96.69	1.56	96.50	3.36	95.40

Table S1a (given in supplementary section S1) reveals that the combination of 100 ppm AME with 50 ppm of PEG400 resulted in improved efficiency in comparison to AME. Only 100 ppm AME extract dose has shown 96.57% η with the addition of 50 ppm PEG in HCl medium. Table S1b shows that AME performs better with PEG400 in HCl medium. The formulation of 100 ppm AME with 50 ppm PEG was the optimized value of this combination which was verified and screened by weight loss measurement. Henceforth, the study of AME along with PEG400 with their best formulation (100 ppm AME with 50 ppm PEG400) in HCl medium was explored through electrochemical techniques.

Electrochemical measurements

Potentiodynamic polarization measurement

The plots of potentiodynamic polarization (PP) measurements of AME in 0.5 M HCl solution are shown in Fig. 2a, b, c respectively at 303 K, 313 K and 323 K. Figure 2d shows the polarization graphs of AME + PEG400. The Tafel parameters obtained after extrapolation of graphs are summarised in Table 2 for AME and AME + PEG400. When the concentration of AME extract increases, a fall in the current density i_{corr} ($\mu\text{A cm}^{-2}$) values in both anodic and cathodic directions was observed. This indicates the adsorption of the inhibitor layer restricted the movement of oxygen to both anodic and cathodic sites. Also, the extract presence shifted the Tafel plots slightly towards positive potentials than the negative potential. Therefore, it can be concluded that the inhibition of anodic reactions occurs dominantly over the cathodic reactions. The i_{corr} values at 100 ppm AME were $120.16 \mu\text{A cm}^{-2}$ and $42.89 \mu\text{A cm}^{-2}$ at 800 ppm, while the i_{corr} values of AME + PEG400 were $30.59 \mu\text{A cm}^{-2}$.

Table 2 reveals that i_{corr} values decrease raucously in the presence of PEG400 as intensifier with AME as compared to AME alone. This indicated that the addition of inhibitor adversely affected the metal dissolution and hydrogen evolution reactions and redistricted the corrosion kinetics (Alibakhshi et al. 2019). PP electrochemical parameters cathodic and anodic Tafel slopes (β_c and β_a), corrosion potential (E_{corr}), corrosion rate (CR) and

Fig. 2 Polarization curves for AME in 0.5 M HCl at **a** 303 K, **b** 313 K, **c** 323 K, **d** AME + 50 ppm PEG

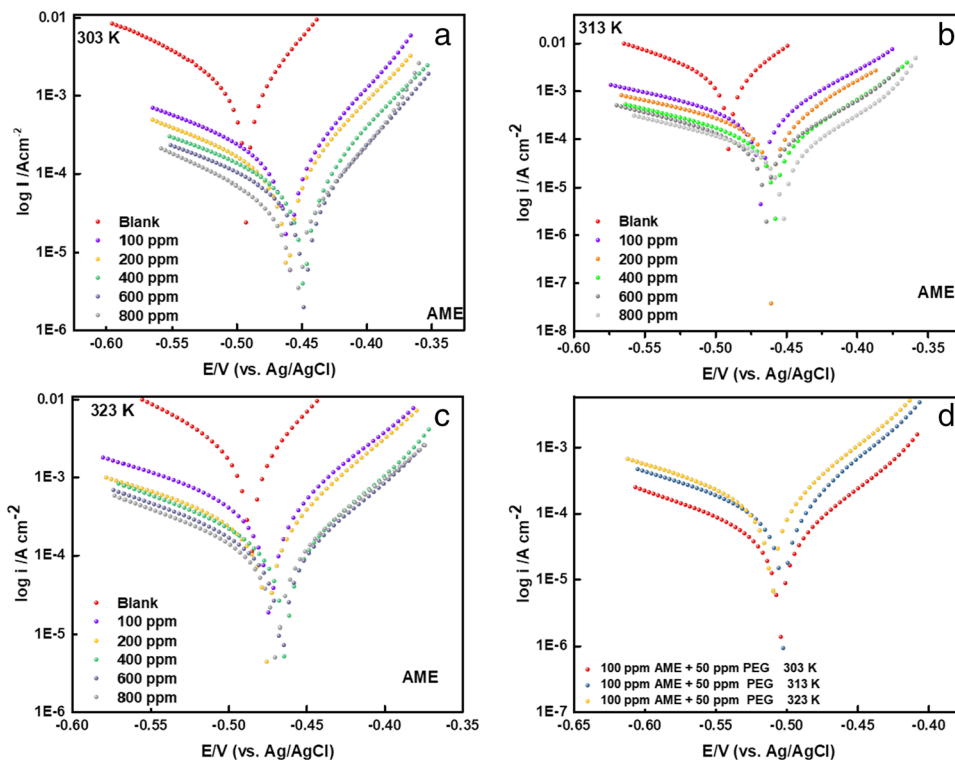
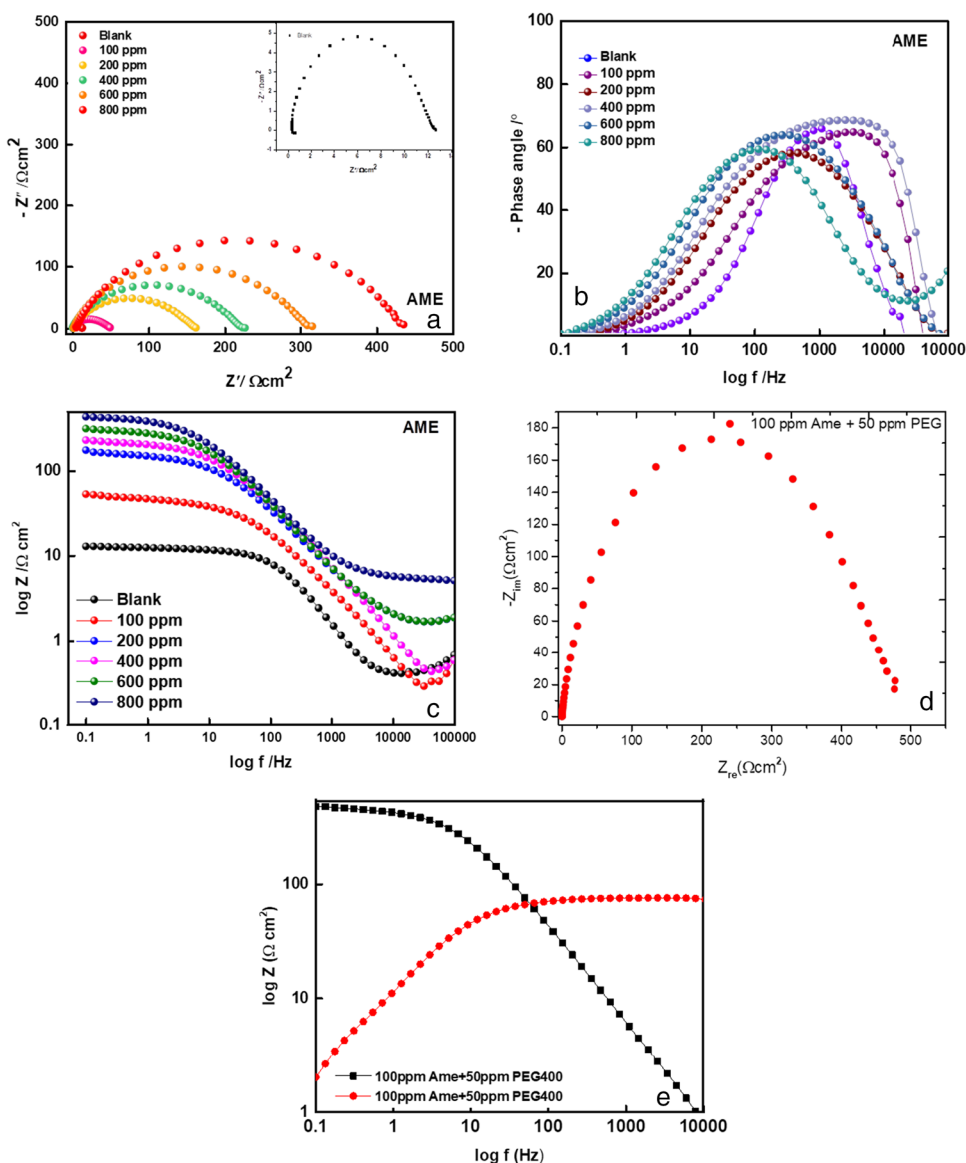


Table 2 Polarization parameters for Fe–C in 0.5 M HCl at different concentration of AME and (AME+PEG400) at 303 K, 313 K, 323 K

C AME/ppm	PEG400/ppm	β_a /mv dec ⁻¹	$-\beta_c$ /mv dec ⁻¹	$-E_{corr}$ vs. Ag/AgCl	$I_{corr}/\mu\text{Acm}^{-1}$	Corrosion Rate/ mmy ⁻¹	Polarization resistance/ Ω	η %
303 K								
0	–	112.73	61.57	492.41	1225.1	14.23	14.11	–
100	–	117.38	58.17	459.64	120.16	1.4	140.58	90.19
200	–	129.56	62.4	460.72	93.21	1.08	196.23	92.39
400	–	111.02	52.14	449.41	51.39	0.59	299.81	95.81
600	–	126.72	63.72	447.46	43.83	0.51	420.08	96.42
800	–	129.69	70.94	504.57	42.89	0.498	464.31	96.57
100	50	102.71	64.34	455.4	30.59	0.36	581.41	97.51
313 K								
0	–	94.38	59.33	490.2	1874.1	21.77	8.44	–
100	–	140.99	65.45	467.67	260.11	3.02	74.63	86.12
200	–	125.03	54.88	460.51	143.34	1.67	115.56	92.34
400	–	120.09	64.58	458.05	84.1	0.98	219.34	95.51
600	–	122.25	73.03	464.32	78.86	0.9512	201.2	95.67
800	–	119.8	55.5	452.43	79.17	0.92	250.8	95.77
100	50	135	70.37	502.5	56.89	0.66	353.11	96.96
323 K								
0	–	98.69	65.99	485.82	2122.6	24.66	8.09	–
100	–	146.22	71.33	473.32	359.47	3.18	57.12	83.06
200	–	143.42	64.65	475.08	213.53	2.48	90.64	89.94
400	–	116.57	69.67	463.56	124.81	1.45	151.76	94.11
600	–	128.14	77.09	465.85	122.83	1.42	148.25	94.21
800	–	118.19	62.56	469.22	119.9	1.39	186.82	94.32
100	50	130.54	73.28	510.29	85.3	1.22	193.59	96.08

Fig. 3 Plots for AME in 0.5 M HCl **a** Nyquist Plots, **b** Bode phase plots **c** Bode modulus. Plots for (AME+PEG400) **d** Nyquist plots, **e** Bode plots



corrosion current density (i_{corr}) are summarized in Table 2. The free electrons available from oxygen, nitrogen and π -electrons help in suppressing the corrosion process by blocking the active sites present over the metal surface

(Saini et al. 2019). The similar patterns followed by Tafel curves indicated no change in the basic corrosion control mechanism over MS surface. However, the displacement of E_{corr} of inhibitor within the range of 85 mV from the

Table 3 EIS parameters and inhibition efficiency value in the absence and presence of AME and (AME+PEG400) at 303 K in 0.5 M HCl

Conc.(ppm) AME	Conc. ppm (PEG400)	R_{CT} (Ω cm ²)	C_{dl} (μ F cm ⁻²)	$CPE/Y_0 \times 10^6 / S$ cm ⁻² S ⁿ²	n	χ^2	η %
Blank	0	12.11	114.2	137.1	0.980	0.840	
100	0	162.42	61.3	94.6	0.995	0.174	92.54
200	0	226.05	58.4	57.6	0.831	1.254	94.64
400	0	303.89	57.5	80.7	0.883	2.970	96.01
600	0	313.93	55.7	77.1	0.909	0.117	96.14
800	0	430.25	53.9	63.3	0.995	0.264	97.18
100	50	476.94	49.09	56.1	0.996	0.247	97.46

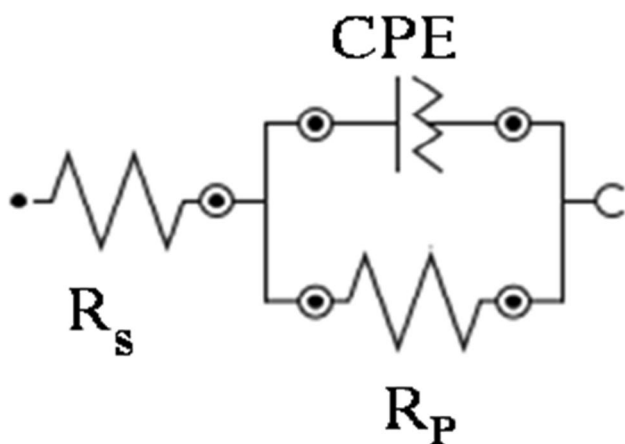


Fig. 4 Electrochemical circuit fit

E_{corr} of blank solution categorized AME as a mixed-type inhibitor. The percentage η was calculated using the relation (Qiang et al. 2017):

$$\eta\% = \frac{i_{corr}^0 - i_{corr}}{i_{corr}^0} \times 100 \tag{3}$$

where i_{corr}^0 and i_{corr} are the current densities of corrosion for MS without and with inhibitor, respectively.

The inhibition efficiency of AME at 100 ppm was 90.19% at 303 K which declined to 83.06% at 323 K. On the other side, η % of AME at 100 ppm along with merely 50 ppm PEG400 was 97.51% at 303 K and 96.08% at 323 K. This depicted the presence of low dosage of PEG400 elevated the inhibition efficiency of AME which may be due to the complexation with MS surface which could sustain the adsorbability of AME even at higher temperatures.

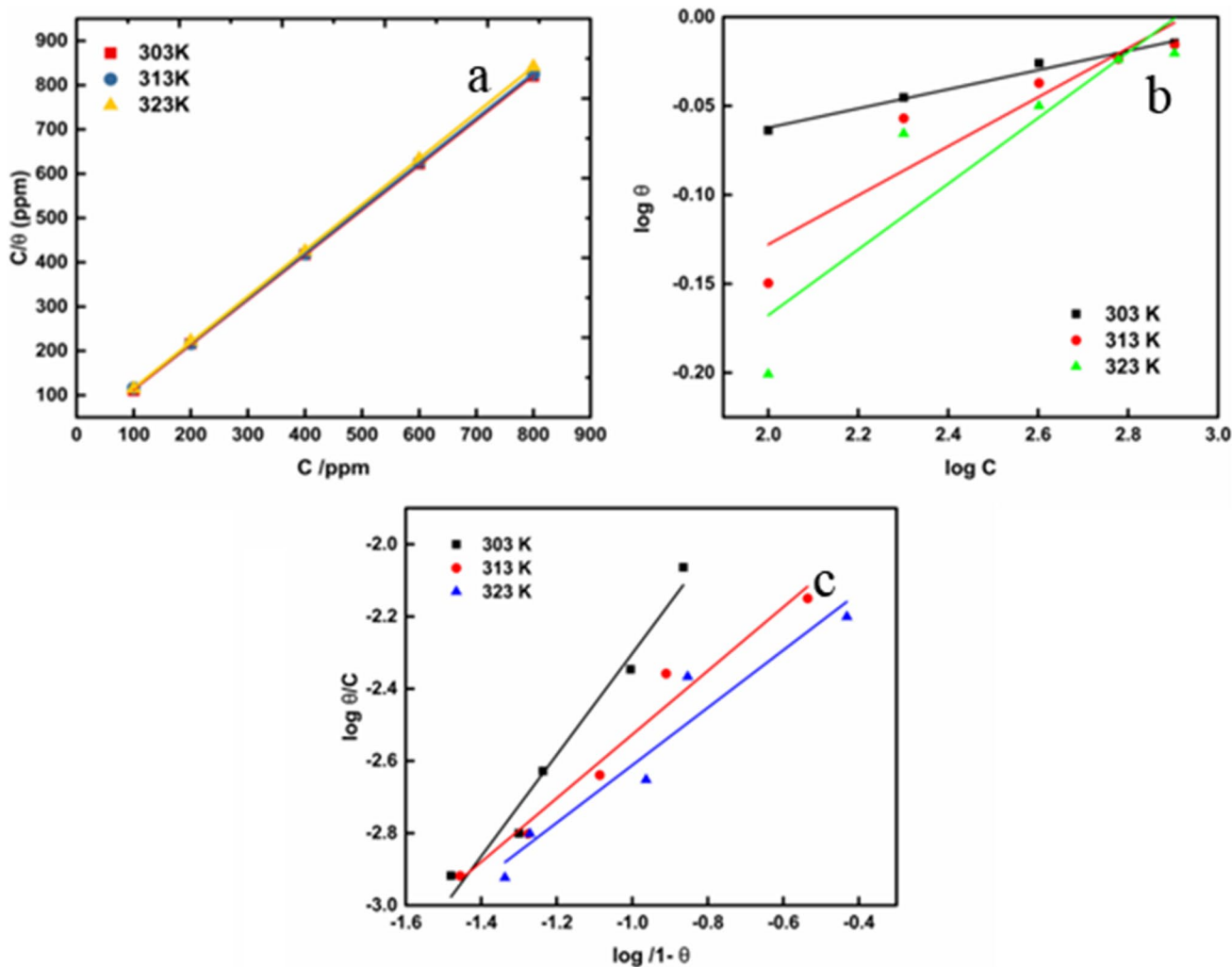


Fig. 5 Adsorption isotherms a Langmuir, b Freundlich, and c Flory–Huggins plots of AME for Fe–C in 0.5 M HCl

Table 4 Thermodynamic adsorption parameters of AME for Fe–C in 0.5 M HCl

Temperature (K)	ΔG°_{ads} (kJ mol ⁻¹) 0.5 M HCl	ΔH°_{ads} (kJ mol ⁻¹) 0.5 M HCl	ΔS°_{ads} (J mol ⁻¹ K ⁻¹) 0.5 M HCl
303 K	-28.25	09.14	39.96
313 K	-27.54		38.69
323 K	-27.57		41.51

EIS

The Nyquist plots of AME and AME + PEG400 at 303 K for the steel in 0.5 M HCl medium are shown in Fig. 3. Figure 3a shows Nyquist plots, Fig. 3b exposes Bode phase, and Fig. 3c depicts Bode modulus of AME in 0.5 M HCl respectively. Figure 3d displays Nyquist plots and Fig. 3e informs about Bode plots for the formulation AME + PEG400 in 0.5 M HCl solution. The capacitive diameter size for AME was noticeably improved in the presence of intensifier PEG400 as compared to that of AME alone. The indication of similar capacitive loops in all cases revealed that the similar mode of inhibition against corrosion was followed

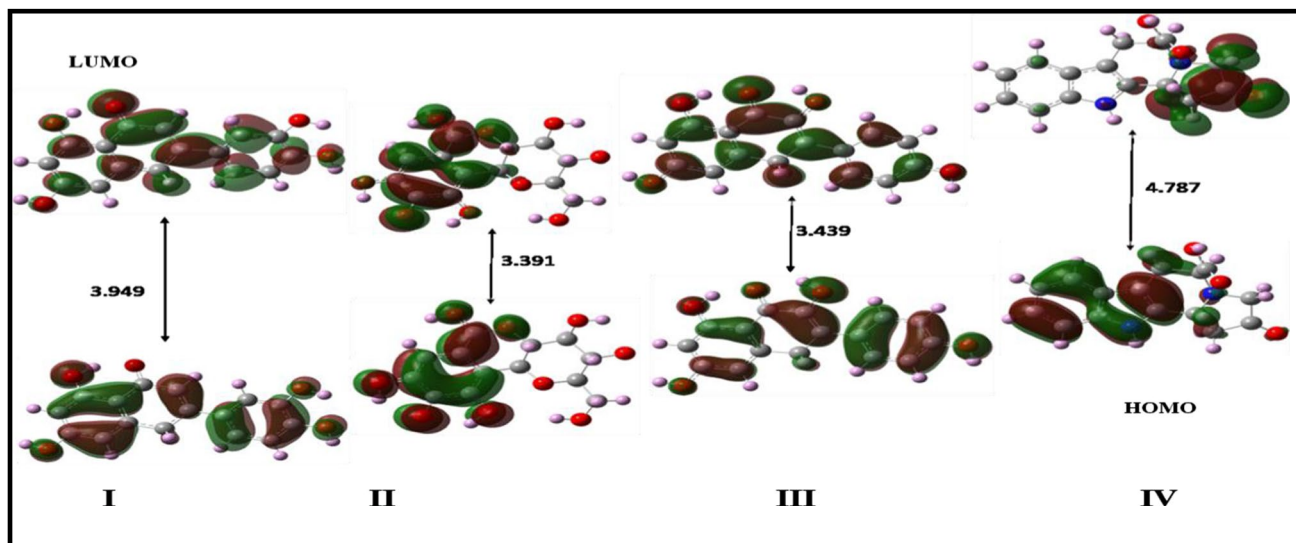
on the MS surface in hydrochloric acid solution. The difference in the values of impedance at low and high frequencies depicted the value of charge transfer resistance (R_{CT}). The frequency-impedance response of MS is directly related to the concentration of the inhibitor (Qiang et al. 2019a, b). The higher values of R_{CT} as compared to the blank solution facilitated that the blocking of active sites over the MS surface occurred effectively through protective/barrier film of inhibitors during adsorption on MS surface.

Based on EIS, the percentage inhibition efficiency ($\eta\%$) and double-layer capacitance (C_{dl}) were analysed using the following equations:

$$\eta\% = \frac{R_{CT} - R_{CT}^0}{R_{CT}^0} \times 100 \quad (4)$$

$$C_{dl} = \frac{1}{2\pi f_{max} R_{CT}} \quad (4.1)$$

where R_{CT} and R_{CT}^0 are the values of charge transfer resistance with and without inhibitor, respectively (Dahiya et al. 2016). A downfall of the C_{dl} values while moving towards higher concentrations of the AME as well as AME with

**Fig. 6** Active constituents quercetin (I), cuscutin (II), kaempferol (III) and cuscutamine (IV) with their *HOMO* and *LUMO* orbital distribution**Table 5** The quantum parameters of quercetin (I), cuscutin (II), kaempferol (III) and cuscutamine (IV)

Molecule	E_{HOMO} (eV)	E_{LUMO} (eV)	ΔE (eV)	Dipole moment (Debye)	Electro negativity (χ) (eV/mol)	Hardness I (eV/mol)	Soft ness σ	ΔN
I	-5.795	-1.846	3.949	6.66	3.82	1.975	0.507	0.253
II	-5.546	-2.155	3.391	4.02	3.85	1.695	0.59	0.286
III	-5.437	-1.999	3.439	4.01	3.72	1.719	0.582	0.32
IV	-5.412	-0.625	4.787	2.02	3.02	2.394	0.418	0.376

PEG400 was also observed. This took place by the replacement of water molecules at the metal/solution interface that resulted in descending pattern of the local dielectric constant along with the consequent adsorption of inhibitor layer (Qiang et al. 2019a, b).

The frequency with the maximum phase angle keeps on increasing along with the addition of inhibitor concentration. The highest phase angle was observed by the addition of PEG with AME. Table 3 indicates the value of η % of AME is shifted from 92.54% at 100 ppm to 97.18% at 800 ppm while only 100 ppm of AME plus 50 ppm of PEG400 provided 97.46% inhibition efficiency. The results are directed towards the retardation of charge transfer with the effectual adsorption of AME along with PEG400 in the HCl medium. The electrochemical equivalent circuit was fitted to examine the EIS parameter as shown in Fig. 4.

Accordingly, a constant phase element (CPE) was utilized to view a more accurate fit of experimental parameters, in spite of a capacitive element which could build normally more complex equivalent circuits, where charge transfer or polarization resistance is R_p , n = value of the exponent of constant phase element and varies from 0, 0.5, 1, - 1 as related with resistance, Warburg impedance, capacitance and inductance, respectively. The uncompensated solution resistance = R_s , CPE = constant phase element, can be calculated by Eq. 5 (Kumar et al. 2017a, b):

$$Z_{CPE} = \left(\frac{1}{Y_0}\right) [(j\omega)^n]^{-1} \tag{5}$$

Table 6 Energy interactions parameters of quercetin (I), cuscutin (II), kaempferol (III) and cuscutamine (IV) as calculated by MD simulation

Fe surface with	Temperature 303 K	
	$E_{interaction}/kJmol^{-1}$	$E_{binding}/kJmol^{-1}$
I	-218.36	218.36
II	-209.74	209.74
III	-448.35	448.35
IV	-109.70	109.70

where, Y_0 = magnitude of CPE, ω = angular frequency, j = imaginary number, and n = exponential term of CPE.

The following relations (Qiang et al. 2022) (Li et al. 2021) are used to convert CPE to C_{dl} :

$$C = Y_0(\omega)^{n-1} = Y_0(2\pi f_{Zim-Max})^n \tag{6}$$

Here, $f_{Zim-Max}$ represents the maximum frequency value of imaginary impedance in EIS.

Figure 3b, c and e show the Bode plots recorded for MS in 0.5 M HCl solution at different concentration of Ame and Ame with PEG respectively. The increase in phase angle with enhancement of concentration of inhibitor clearly indicates the inhibition of corrosion reactions. The elevation in the phase angle with increasing inhibitor concentration specifies the reduction in heterogeneity of the surface. An aliquoted addition of inhibitor may be directly associated with surface smoothness through compact

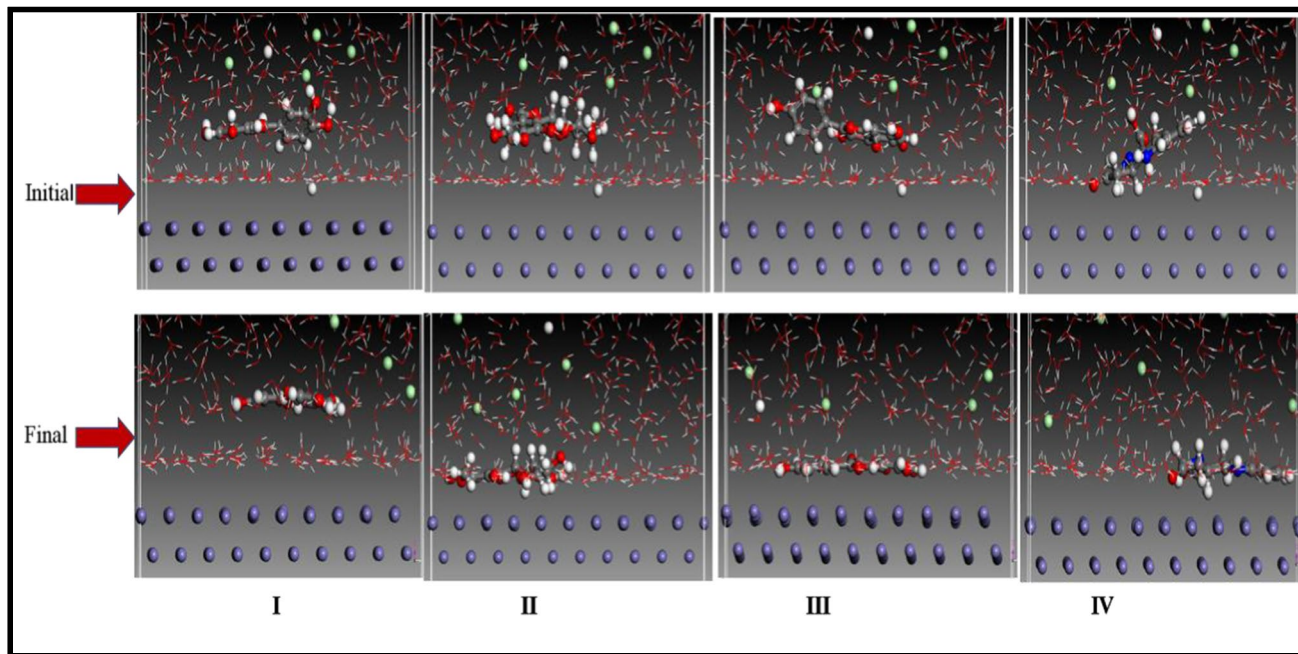


Fig. 7 MD simulation orientation with initial and final view for quercetin (I), cuscutin (II), kaempferol (III) and cuscutamine (IV)

adsorption of inhibitor molecules over the metal surface.

Adsorption and thermodynamic aspects

The basic idea about the mechanism of adsorption and interaction between MS surface and the examined compounds can be predicted through adsorption isotherms. The basic concept of surface coverage (θ) can be given through Eq. 7:

$$\theta = \frac{\eta}{100} \quad (7)$$

Here, η is the inhibition efficiency.

The Langmuir adsorption isotherm (Fig. 5a) analysis reveals that the plots of C/θ versus C represent ideal correlation coefficient ($R^2 \geq 0.99$) which is given by Eq. 8:

$$\frac{C}{\theta} = \frac{1}{K_{ads}} + C \quad (8)$$

Here, C is the concentration of AME, and K_{ads} is the equilibrium constant which can be evaluated from the intercept of the plot of C/θ versus C . The K_{ads} is used to calculate thermodynamic parameters (ΔH°_{ads}) (Ayawei et al. 2017). The graph of $\ln K_{ads}$ versus $1/T$ gives a straight line (Fig. S2 placed in supplementary section S2) with slope ($-\Delta H^\circ_{ads}/R$) from which ΔH°_{ads} and ΔS°_{ads} thermodynamic parameters were analysed (Table 4). Moreover, to predict the mutual influence of PEG400 and AME towards the inhibition action of corrosion, the synergism parameter, S_θ , was premeditated using the relationship (Alibakhshi

et al. 2019) (as placed in supplementary section S3). Freundlich isotherm (Fig. 5b) and Flory–Huggins adsorption isotherms (Fig. 5c) were determined, and their respective parameters are placed in Table S3 to give more insight in the adsorption process; further explanation is placed in supplementary section S4.

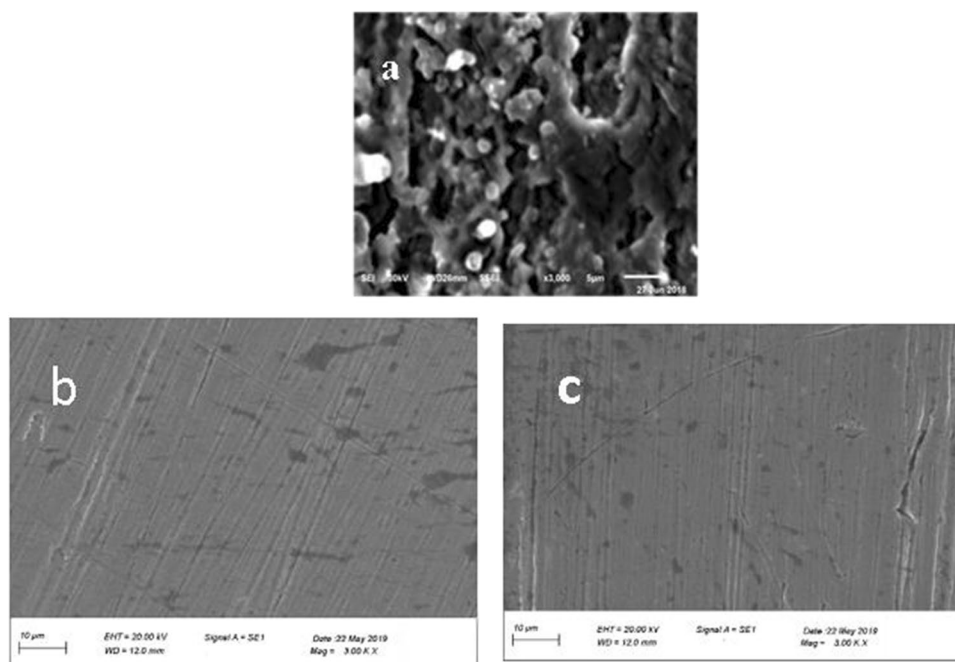
Computational (DFT and MD) study

Herein, Fig. 6 puts insight into the electronic and structural properties of active constituents of AME, i.e. quercetin (I), cuscutin (II), kaempferol (III) and cuscutamine (IV).

The corresponding calculated quantum chemical parameters in Table 5 display the quantum parameters such as; E_{HOMO} , E_{LUMO} , ΔE , the fraction of electrons transferred (ΔN), electronegativity (χ) and absolute hardness (I) (Eddy et al. 2015) (Kokalj 2014).

The highest E_{HOMO} value of quercetin among active constituent denotes that it has the highest tendency for electron donation to an electron-deficient site. The reactivity of the molecule is inversely related to the value of ΔE since its smaller value enhanced the softness of the molecule and its easy polarizability (Majd et al. 2019). The positive values for ΔN confirm that all active constituents exhibit the propensity to donate electrons to the metal surface. The ΔN values in quercetin, cuscutin, kaempferol and cuscutamine follow the order 0.25, 0.28, 0.32 and 0.37 respectively. This displays the extent of electron fraction transferred from cuscutamine is higher and which further validated through the least electronegative ($\chi = 3.02$ eV) value of cuscutamine among the active constituents. The polarity of a molecule is related to

Fig. 8 Scanning electron micrographs of Fe–C surfaces: **a** inhibited AME and **b** inhibited (AME + PEG400)



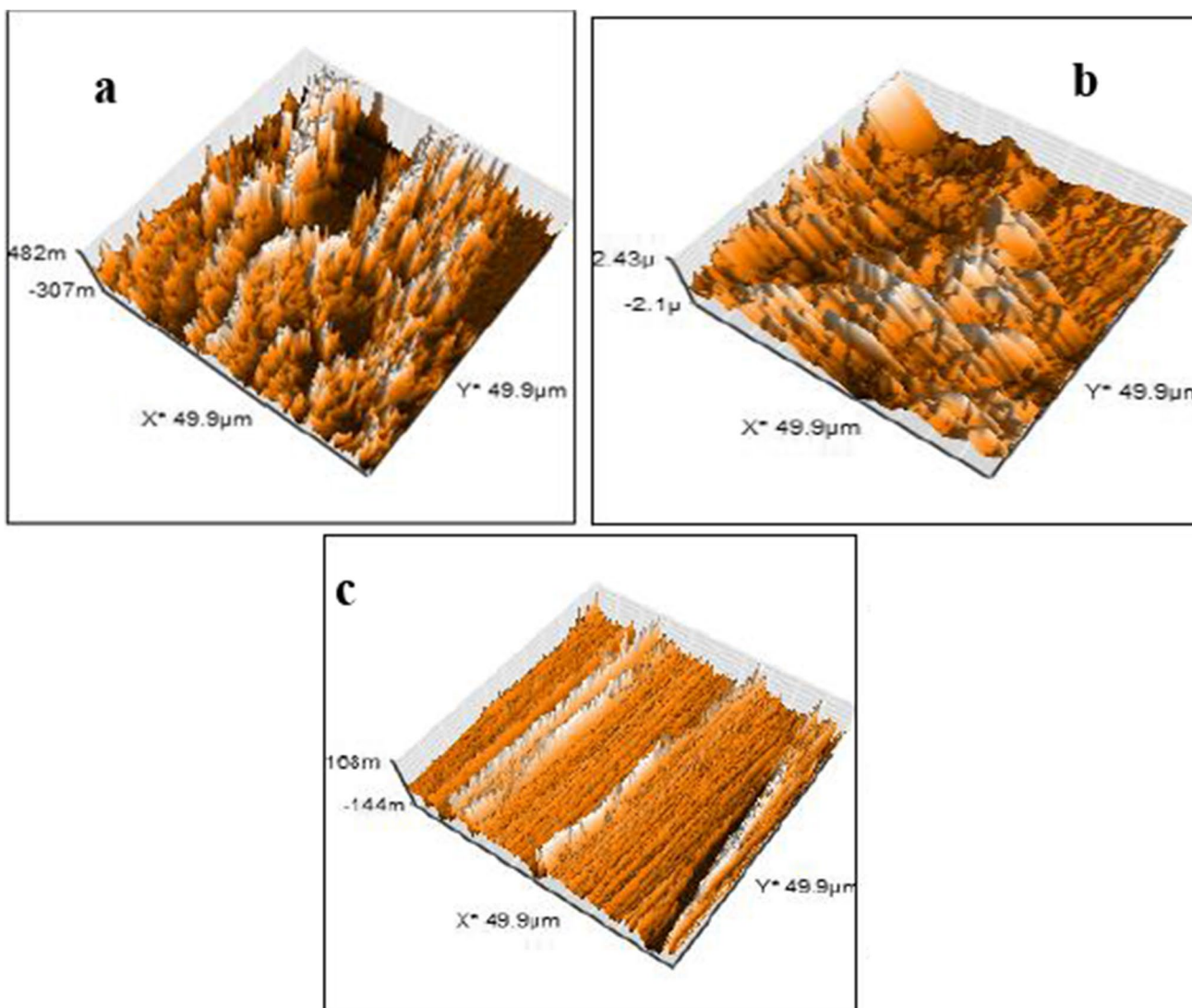


Fig. 9 Atomic force micrographs of Fe–C surfaces: **a** 0.5 M HCl, **b** AME inhibited, and **c** AME + PEG400 inhibited

the product of charge and the distance between two related atoms. Though the dipole moments of all the species are quite sufficient for the existence of electrostatic interactions at the metal/solution interface, quercetin possesses the highest value of dipole moment. Analysis of an assortment of parameters gives a deep understanding of the interaction of

the metal surface with an inhibitor (Kokalj 2014). It is reasonable to propose that all the active constituents contribute good inhibitive effects against corrosion as a result of mutual synergism among them. Hence, Table 5 results evidenced the fact that the major constituents of AME facilitated the electron density donation towards iron metal and eventually protected the metal surface.

MD is a powerful simulation tool to study the adsorption interactions of inhibitor on the Fe surface (Qiang et al. 2021). The type of functional groups, electron donor site and size of inhibitors are the deciding factors for energy binding interface between inhibitors and metal surface. In relevance to this, MD of the studied inhibitors with their initial and final adsorption orientation on the Fe surface are depicted and are shown in Fig. 7. The figure clearly shows that quercetin (I) and

Table 7 Roughness parameters obtained for Fe–C surface through AFM

Inhibitor	Line roughness(nm)	Area roughness(nm)
Blank 0.5 M HCl	587.78	917.73
0.5 M HCl+ AME	172.24	505.13
0.5 M HCl+ AME + PEG400	121.71	167.63

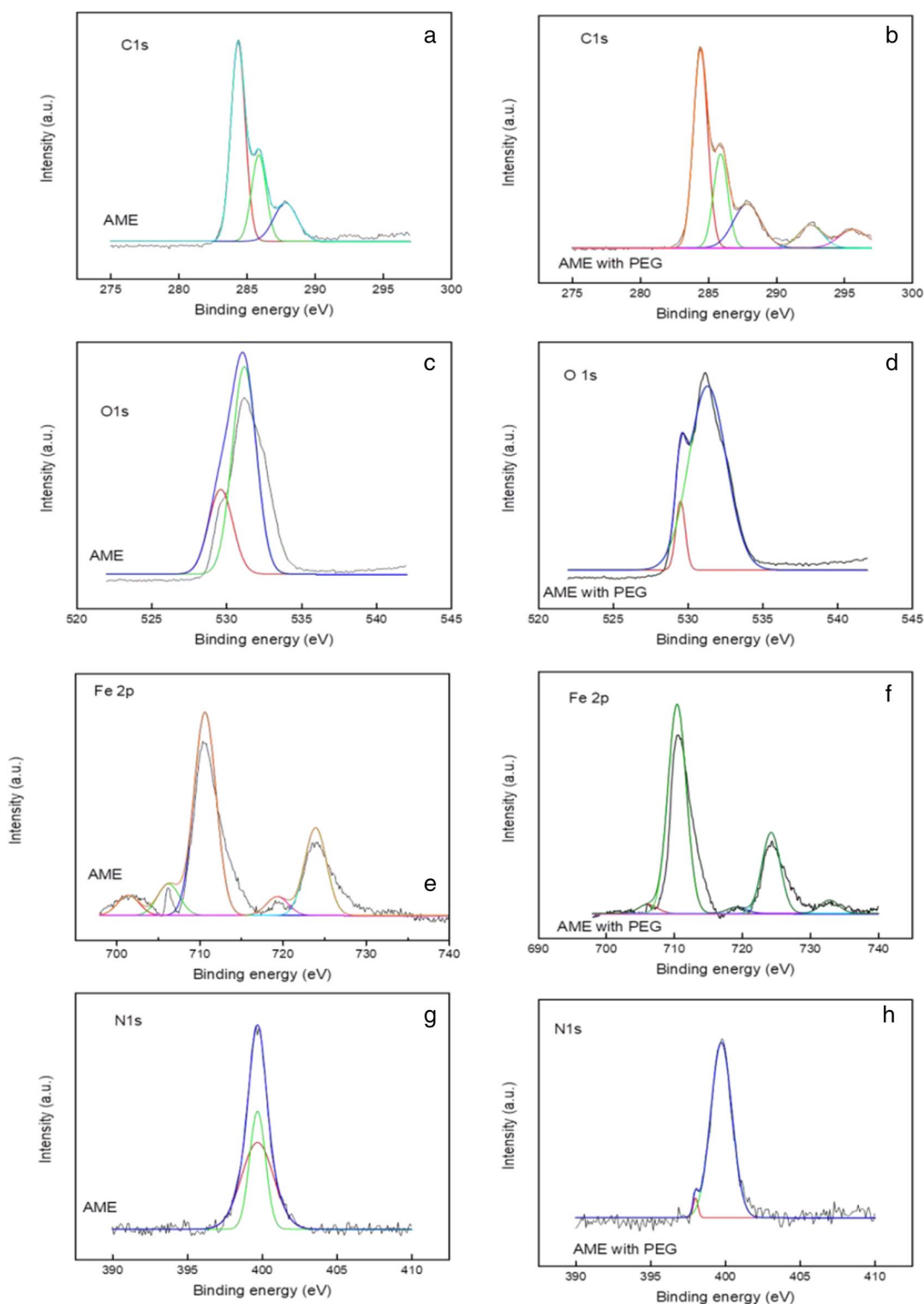


Fig. 10 XPS spectra of Fe–C surface after immersion in AME and AME with PEG

kaempferol (III) were adsorbed to greater extent than cuscutin (II), cuscutamine (IV) on Fe surface. The presence of hydroxyl group, quinoline nucleus and imine groups favoured the planar orientation on metal surface.

Table 6 exposes the energy parameters of the studied inhibitors. The negative values of binding energy support and strengthen the interactions between inhibitors with metal surface.

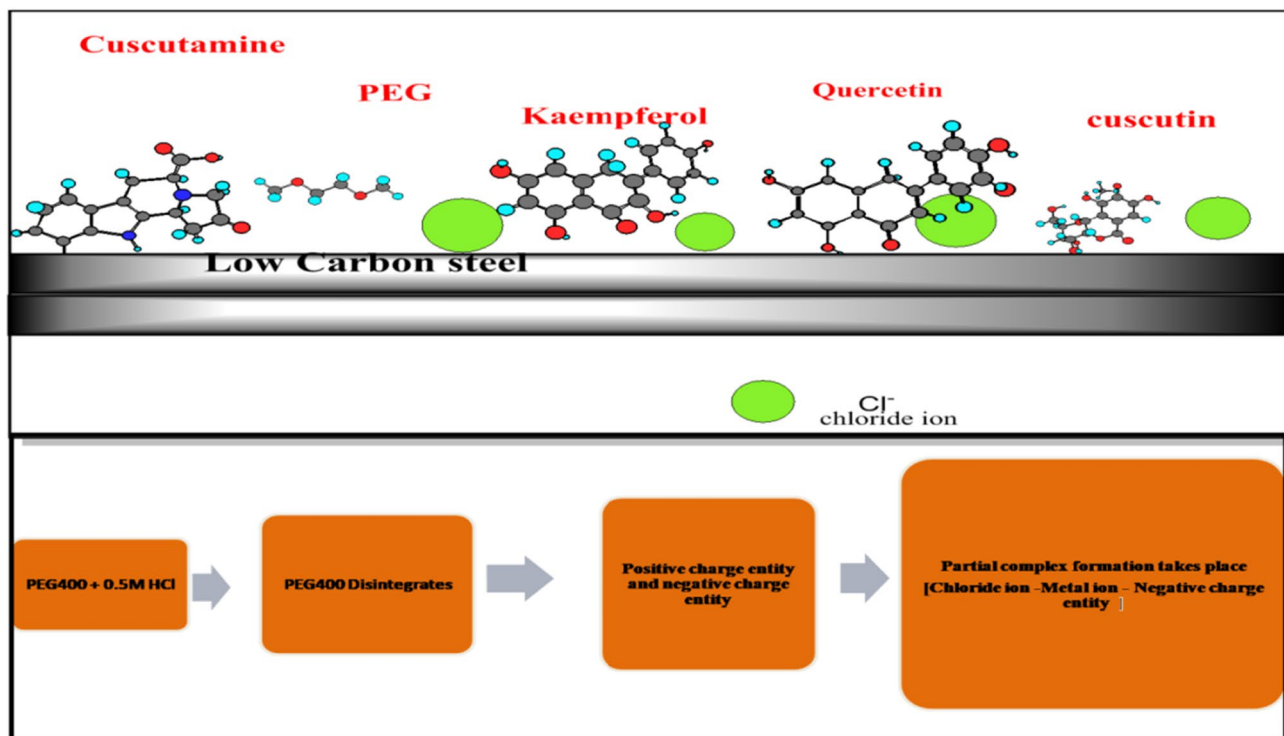


Fig. 11 Proposed mechanism of inhibitor AME with intensifier

SEM study

Typical scanning electron microscopy (SEM) photographs of the surfaces at $\times 3000$ magnification after immersion of 4 h in 0.5 M HCl at 303 K without and with 800 ppm AME concentration and (100 ppm AME + 50 ppm PEG400) concentration are shown in Fig. 8a, b and c. The surface appears the most heterogeneous, rough, by the attack of corrosive HCl in Fig. 8a. The morphology in the presence of AME + PEG400 formulation reveals that the MS steel surface is more protected as compared to AME alone. Figure 8c exposes a smoother, non-porous and less disintegrated structure than Fig. 8b. Hence, SEM proves adsorption of the inhibitor AME + PEG400 layer acted as an effective barrier against electrochemical corrosion reactions occurring on the MS surface in the corrosive solution.

AFM

The MS surface microstructure in 0.5 M HCl medium at 303 K before and after immersion in the presence of AME and the combination of AME with PEG400 for 4 h was recorded using AFM (Fig. 9). Figure 9a shows a highly corroded surface in the presence of the purely acidic medium. The presence of corrosion controlling candidates makes the surface of steel relatively homogeneous, plane, compressed

as shown in Fig. 9b (AME) and Fig. 9c (AME + PEG400). The roughness parameters in Table 7 indicate about the prominent surface improvement within AME with PEG400 in comparison to AME alone, both studied in 0.5 M HCl medium.

XPS

X-ray photoelectron spectroscopy (XPS) study was executed to analyze the interaction of the inhibitor with the metal surface and to insight the type of elements of extract existing on the surface of metal. Figure 10 shows the deconvoluted C1s, O1s and Fe 2p spectrum of Ame and Ame with PEG inhibitors, and the same was compared with the XPS spectrum of blank solution given in our previous paper (Pahuja et al. 2020) and added in supplementary section S5.

Figure 10a and b show the high-resolution spectra of C1s region of metal surface with inhibitors. The binding energy peaks observed for the C1s spectra correspond to different oxidation states of carbon. The peak at 284.87 eV was observed due to aromatic C–C and C=C. The peak at 285.63 eV was attributed to C=O bonds in the molecule whereas the peak at 288 eV corresponding to the presence of $-(C=O)-O-$ relates to the cyclic carboxylic ester. The tiny peak at 286.65 corresponds to CH–NH bonding.

Table 8 Summarized comparative data with the present study

Corrosion inhibitor	Corrosive matrix	Conc	Techniques used	Highest efficiency $\eta/\%$	Solvent used for extraction	Recent publications
<i>Rosa canina</i> fruit extract	1 M HCl	800 ppm	EIS, potentiodynamic polarization	86	Water	Sanaei et al. (2019)
<i>Biden pilosa</i>	1 M HCl	0.5 g/L	Weight loss method, potentiodynamic polarization	97	Ethanol	Olusegun et al. (2018)
<i>Peganum harmala</i>	1 M HCl	800 ppm	Weight loss method, potentiodynamic polarization	95	Water	Bahlakeh et al. (2019)
Ginko leaf extract	1 M HCl	2000 ppm	EIS, potentiodynamic polarization	92	Water, ethanol	Qiang et al. (2018)
Phuinam Extract	1 M HCl	0.4 g/L	Weight loss, EIS, potentiodynamic polarization	95	Methanol	Prakash et al. (2018)
<i>X. strumarium</i> extract	1 M HCl	10 ml/L	Weight loss	94	HCl	Khadom et al. (2018)
<i>Mangifera indica</i> leaves	1 M HCl	1000 ppm	EIS, potentiodynamic polarization	92	Ethanol	Ramezanzadeh et al. (2018)
<i>Primula vulgaris</i> extract	1 M HCl	1000 ppm	EIS, potentiodynamic polarization	95	Water	Majd et al. (2019)
Ricestraw extract	3.5% NaCl	1.5 g/L	Weight loss	92	Ethanol	Othman et al. (2019)
<i>Bistorta officinalis</i>	Simulated cooling water	1000 ppm	Weight loss EIS, potentiodynamic polarization	93	Methanol	Mohammadi and Rahsepar (2019)
<i>Persian Liquorice</i>	0.5 M NaCl	600	EIS, potentiodynamic polarization	98		Alibakhshi et al. (2019)
<i>Heterophragma adenophyllum</i> extract	0.5 M HCl	600 ppm	Weight loss EIS, potentiodynamic polarization	98	Ethanol	Pahuja et al. (2020)
Amarbel extract AME	0.5 M HCl	100 ppm + 50 ppm PEG400	Weight loss EIS, potentiodynamic polarization	97	Ethanol	Present study

Figure 10c and d display the deconvoluted O1s spectra; peaks at 529.82 eV in AME and 529.62 eV in AME with PEG relate to O^{2-} and indicate the presence of ferric oxides (Fe_2O_3 and Fe_3O_4). The interpretation of these peaks clearly points to the enhancement in the inhibitive action of AME in the presence of PEG. The peaks at 531.32 eV in AME and 531.77 eV in AME with PEG were attributed to OH^- of hydrous iron oxide $FeOOH/Fe(OH)_3$. The weak peak at 533.82 eV with lower binding energy indicates the existence of water molecules as monolayer (Qiang et al. 2019a, b) (Hashim et al. 2019a).

Figure 10e and f expose Fe 2p spectrum of inhibitors suggest the presence of various forms of oxidized iron with metallic iron. The spectrum covers a doublet peak profile positioned at a binding energy around 710.96 eV ($Fe\ 2p_{3/2}$) and 724.83 eV ($Fe\ 2p_{1/2}$). The peaks at 708.57 eV ($Fe\ 2p_{3/2}$) and 721.88 eV ($Fe\ 2p_{1/2}$) were allocated for metallic Fe(0). The peaks at 711.62 eV ($Fe\ 2p_{3/2}$) and 725 eV ($Fe\ 2p_{1/2}$) were attributed to the Fe^{2+} (Fe_3O_4 or FeO) and the peaks 713.7 eV ($Fe\ 2p_{3/2}$) and

727.38 eV ($Fe\ 2p_{1/2}$) correspond to Fe^{3+} (Fe_2O_3). The peaks residing at lower side of binding energy were related with Fe^{2+} which arose as a result of the metal dissolution after immersion in corrosive HCl. The peaks at 718.4 eV, 721.8 eV, 733.4 eV and 735.3 eV were assigned as satellite peaks of $Fe\ 2p_{3/2}$ and $Fe\ 2p_{1/2}$ (Hashim et al. 2019b) (Grosvenor et al. 2004). The typical spectra N1s are shown in Fig. 10g and h, corresponding to the characteristic fitted peaks at 399.5 eV and 401 eV. This shows the presence of adsorbed nitrogen components of the extract on mild steel.

The interpretation of XPS peaks confirms that the adsorbed film of Fe_2O_3 and $FeOOH$ retards the ionic diffusion and prevents the corrosion of metal surface more efficiently in the presence of AME with PEG.

Mechanism strategy for corrosion protection

The adsorptive nature of the studied compounds over MS steel surface is found supportive in preventing the

corrosion in acidic medium. The surface coverage through adsorption precisely depends upon the electronic structure and composition of metal, inhibitor and corrosive medium. The various active compounds present in the Amarbel extract possess organic nature, rich with flavonoids, aromatic rings, tannins, carbohydrate, proteins and electron donor heteroatom. In acidic conditions, these compounds get protonated and reduce the hydrogen evolution at the cathodic sites of MS surface whereas the adsorption of molecules at anodic sites through electron-rich centre decreased the dissolution rate of the metal. The mode of action of studied inhibitors is represented in Fig. 11.

In addition to this, the inhibition takes place effectively even at a low concentration of PEG400 when HCl was used as a corrosive medium. As some molecules of PEG400 may also get disintegrated into positive and negative entities, later on, the metal ion gets entrapped as partial complexation between this negative entity of PEG400 and chloride ions.

Eventually, Table 8 summarizes some current literature related with plant extract as corrosion inhibitors. The corrosion inhibitors should be used at concentrations between range 0.1 and 1%. Low concentration of Ame with intensifier is fulfilling the conditions of a good inhibitor as compared to the other inhibitors present in Table 8.

Conclusions

The current study informs about the anti-corrosive strength of the alcoholic extract of Amarbel extract (AME) alone and the combination of polyethylene glycol (PEG400) as additive with AME in 0.5 M HCl solution onto MS steel surface. The results obtained through weight loss, electrochemical polarization and impedance techniques were found mutually in good harmony. The examination of results indicates that the combination of AME at 100 ppm concentration with 50 ppm PEG400 has elevated the corrosion inhibition efficiency up to 97%. The presence of PEG400 was helpful in maintaining the inhibition efficiency of AME at low dosage (100 ppm) even at higher temperatures in a stable manner. Potentiodynamic polarization findings support AME as well as AME + PEG400, both acted as mixed-type corrosion inhibitors for MS surface. The Langmuir, Freundlich and Flory–Huggins adsorption isotherms, XPS, SEM AFM and computational study have supported the corrosion inhibition capability of the studied eco-friendly inhibitors over the MS surface in a justified way and also aided with a proposed strategy for mechanism of inhibition while working in 0.5 M HCl.

Supplementary Information The online version contains supplementary material available at <https://doi.org/10.1007/s11356-022-23842-8>.

Author contribution All the authors contributed to the study conception and design.

Priti Pahuja: conceptualization; data curation; funding acquisition; investigation; methodology; resources; validation; roles/writing — original draft.

Meena Yadav: formal analysis, data curation, resources.

Monika Dhanda: formal analysis, data curation, resources.

Rajat Arora: formal analysis, data curation, resources.

Simran Ahlawat: formal analysis, data curation, resources.

Ajay Satija: formal analysis, data curation, resources.

Neeru Jhanjhariya: formal analysis, data curation, resources.

Sumit Kumar: supervision; formal analysis, investigation, validation; visualization; writing — review and editing.

Suman Lata: conceptualization; supervision; methodology; formal analysis, investigation, validation; visualization; writing — review and editing.

Funding The Council of Scientific and Industrial Research, New Delhi, India, awarded fellowship to Meena Yadav (award letter no. 09/1063(0028)/2019-EMR-I); University Grant Commission (UGC), Delhi, provided fellowship to Monika Dhanda (Ref. No. 201610158088) and Neeru Jhanjhariya (Ref. No. 153) as JRF.

Deenbandhu Chhotu Ram University of Science and Technology, Murthal, provided Rajat Arora and Simran Ahlawat, University Research Scholarship (Endst. No. DCRUST/Sch./2019/508) and (Endst. No. DCRUST/Sch./2021/218–223).

Data availability Supplementary data and material will be published as received from the author.

Declarations

Ethical approval The research submitted is carried out in compliance with relevant institutional biosafety and biosecurity protocols.

Consent to participate Informed consent was obtained from all individual participants included in the study.

Consent for publication The authors affirm that participants provided informed consent for publication of all images in the figures.

Competing interests The authors declare no competing interests.

References

- Abdullah Dar M (2011) A review: plant extracts and oils as corrosion inhibitors in aggressive media. *Ind Lub Tribol* 63(4):227–233
- Afia L et al (2015) Electrochemical evaluation of linseed oil as environment friendly inhibitor for corrosion of steel in HCL solution. *Port Electrochim Acta* 33(3):137–152
- Ahmad A, Tandon S, Dang T, Nooreen Z (2017) ScienceDirect a review on phytoconstituents and biological activities of *Cuscuta* species. *Biomedicine Et Pharmacotherapy* 92:772–795
- Alibakhshi E et al (2019) Persian liquorice extract as a highly efficient sustainable corrosion inhibitor for mild steel in sodium chloride solution. *J Clean Prod* 210:660–672
- Arukalam IO et al (2020) Inhibition of sulfate-reducing bacteria influenced corrosion on hydrophobic poly(dimethylsiloxane) coatings. *J Mater Sci Technol* 52:198–206
- Ayawei N, Ebelegi AN, Wankasi D (2017) Modelling and Interpretation of Adsorption Isotherms. *J Chem* 2017:3039817. <https://doi.org/10.1155/2017/3039817>

- Bahlakeh G, Ramezanzadeh B, Dehghani A, Ramezanzadeh M (2019) Novel cost-effective and high-performance green inhibitor based on aqueous *Peganum harmala* seed extract for mild steel corrosion in HCl solution: detailed experimental and electronic/atomic level computational explorations. *J Mol Liq* 283:174–195. <https://doi.org/10.1016/j.molliq.2019.03.086>
- Boudellouia H, Hamlaoui Y, Tifouti L, Pedraza F (2019) Effects of polyethylene glycol (PEG) on the corrosion inhibition of mild steel by cerium nitrate in chloride solution. *Appl Surf Sci* 473:449–460
- Chevalier M et al (2014) Enhanced corrosion resistance of mild steel in 1 M hydrochloric acid solution by alkaloids extract from Aniba Rosaedora Plant: Electrochemical, Phytochemical and XPS Studies. *Electrochim Acta* 131:96–105. <https://doi.org/10.1016/j.electacta.2013.12.023>
- Dahiya S, Suman L, Parmod K, Rajeev K (2016) Original article a descriptive study for corrosion control of low-alloy steel by Aloe vera extract in acidic medium. 34(4): 241–48.
- Dariva CG, Galio AF (n.d.) Corrosion inhibitors – principles, mechanisms and applications
- Deyab MA (2018) Utilization of a nonionic surfactant for improved corrosion resistance of carbon steel in simulated fuel-grade ethanol. *RSC Adv* 8(37):20996–21001
- Eddy NO, Momoh-Yahaya H, Oguzie EE (2015) Theoretical and experimental studies on the corrosion inhibition potentials of some purines for aluminum in 0.1 M HCl. *J Adv Res* 6(2):203–17. <https://doi.org/10.1016/j.jare.2014.01.004>
- El Aoufir Y et al (2017) Corrosion inhibition of carbon steel in 1M HCl by 1,5-benzodiazepine derivative: experimental and molecular modeling studies. *J Mater Environ Sci* 8(6):2161–2173
- Fares MM, Maayta AK, Al-Mustafa JA (2013) Synergistic corrosion inhibition of aluminum by polyethylene glycol and ciprofloxacin in acidic media. *J Adhes Sci Technol* 27(23):2495–2506
- Fazal BR, Becker T, Kinsella B, Lepkova K (2022) A review of plant extracts as green corrosion inhibitors for CO₂ corrosion of carbon steel. *Npj Materials Degradation* 6(1):5. <https://doi.org/10.1038/s41529-021-00201-5>
- Grosvenor AP, Kobe BA, Biesinger MC, McIntyre NS (2004) Investigation of multiplet splitting of Fe 2p XPS spectra and bonding in iron compounds. *Surf Interface Anal* 36(12):1564–1574
- Hashim N, Zakiah N et al (2019a) XPS and DFT investigations of corrosion inhibition of substituted benzylidene schiff bases on mild steel in hydrochloric acid. *Appl Surf Sci* 476:861–77. <https://doi.org/10.1016/j.apsusc.2019.01.149>
- Hashim NZN, Anouar EH, Kassim K, Zaki HM, Alharthi AI, Embong Z (2019b) XPS and DFT investigations of corrosion inhibition of substituted benzylidene Schiff bases on mild steel in hydrochloric acid. *Appl Surf Sci* 476:861–877. <https://doi.org/10.1016/j.apsusc.2019.01.149>
- Kesavan D, Gopiraman M, Nagarajan S (2012) Green inhibitors for corrosion of metals : a review correspondence. *Chem Sci Rev Lett* 1(1):1–8
- Khadom AA, Abd AN, Ahmed NA (2018) Xanthium Strumarium leaves extracts as a friendly corrosion inhibitor of low carbon steel in hydrochloric acid: kinetics and mathematical studies. *S Afr J Chem Eng* 25:13–21
- Kokalj A (2014) Molecular modeling of organic corrosion inhibitors: why bare metal cations are not appropriate models of oxidized metal surfaces and solvated metal cations. *Acta Chim Slov* 61(2):340–349
- Krishnegowda PM, Venkatesha VT, Krishnegowda PKM, Shivayogiraju SB (2013) Acalypha Torta leaf extract as green corrosion inhibitor for mild steel in hydrochloric acid solution. *Ind Eng Chem Res* 52(2):722–28
- Kumar R, Chahal S, Kumar S et al (2017a) Corrosion inhibition performance of chromone-3-acrylic acid derivatives for low alloy steel with theoretical modeling and experimental aspects. *J Mol Liq* 243(August):439–450. <https://doi.org/10.1016/j.molliq.2017.08.048>
- Kumar R, Chahal S, Dahiya S et al (2017b) Experimental and theoretical approach to exploit the corrosion inhibition activity of 3-formyl chromone derivatives on mild steel in 1 m H₂SO₄. *Corros Rev* 35(2):95–110
- Li H, Zhang S, Qiang Y (2021) Corrosion retardation effect of a green cauliflower extract on copper in H₂SO₄ solution: electrochemical and theoretical explorations. *J Mol Liq* 321:114450. <https://doi.org/10.1016/j.molliq.2020.114450>
- Majd MT et al (2019) Green method of carbon steel effective corrosion mitigation in 1 M HCl medium protected by *Primula vulgaris* flower aqueous extract via experimental, atomic-level MC/MD simulation and electronic-level DFT theoretical elucidation. *J Mol Liq* 284:658–674. <https://doi.org/10.1016/j.molliq.2019.04.037>
- Mehdipour M, Ramezanzadeh B, Arman SY (2015) Electrochemical noise investigation of aloe plant extract as green inhibitor on the corrosion of stainless steel in 1M H₂SO₄. *J Ind Eng Chem* 21:318–327
- Mohammadi Z, Rahsepar M (2019) The use of green bistorta Officialis extract for effective inhibition of corrosion and scale formation problems in cooling water system. *J Alloy Compd* 770:669–678
- Naderi R et al (2022) Use of licorice plant extract for controlling corrosion of steel rebar in chloride-polluted concrete pore solution. *J Mol Liq* 346:117856. <https://doi.org/10.1016/j.molliq.2021.117856>
- Olusegun SJ, Okoronkwo EA, Okotete AE (2016) Gravimetric and electrochemical studies of corrosion inhibition potential of acid and ethanol extract of siam weed on mild steel. *Leonardo Journal of Sciences* 29:25–42
- Olusegun SJ, Bodunrin M, Aribo S (2018) Inhibition of mild steel corrosion in HCl solution by plant extract of *Biden pilosa*. *January*. <https://doi.org/10.7537/marsnsj160118.01.Keywords>
- Othman NK, Yahya S, Ismail MC (2019) Corrosion inhibition of steel in 3.5% NaCl by rice straw extract. *J Ind Eng Chem* 70:299–310
- Pahuja P et al (2020) The protection mechanism offered by heterophragma *Adenophyllum* extract against Fe-C steel dissolution at low pH: computational, statistical and electrochemical investigations. *Bioelectrochemistry* 132:107400. <https://doi.org/10.1016/j.bioelechem.2019.107400>
- Prakash J, Shrivastava R, Kumar R (2018) Corrosion Inhibition effect of *Clerodendron Colebrookianum* Walp Leaves (*Phuinam*) Extract on the Acid Corrosion of Mild Steel 1. 1–12. <https://doi.org/10.1134/S2070205118010264>
- Qiang Y et al (2017) Experimental and theoretical studies of four allyl imidazolium-based ionic liquids as green inhibitors for copper corrosion in sulfuric acid. *Corros Sci* 119:68–78
- Qiang Y, Zhang S, Tan B, Chen S (2018) Evaluation of Ginkgo leaf extract as an eco-friendly corrosion inhibitor of X70 steel in HCl solution. *Corrosion Science, January*, 1–11. <https://doi.org/10.1016/j.corsci.2018.01.008>
- Qiang Y, Zhang S, Zhao H, Tan B, Wang L (2019a) Enhanced anticorrosion performance of copper by novel N-doped carbon dots. *Corros Sci* 161(June):108193. <https://doi.org/10.1016/j.corsci.2019.108193>
- Qiang Y, Zhang S, Wang L (2019b) Understanding the adsorption and anticorrosive mechanism of DNA inhibitor for copper in sulfuric acid. *Appl Surf Sci* 492(June):228–238
- Qiang Y, Guo L, Li H, Lan X (2021) Fabrication of environmentally friendly losartan potassium film for corrosion inhibition of mild steel in HCl medium. *Chem Eng J* 406(July 2020):126863. <https://doi.org/10.1016/j.cej.2020.126863>
- Qiang Y, Zhi H, Guo L, Fu A, Xiang T, Jin Y (2022) Experimental and molecular modeling studies of multi-active tetrazole derivative

- bearing sulfur linker for protecting steel from corrosion. *J Mol Liq* 351:118638. <https://doi.org/10.1016/j.molliq.2022.118638>
- Raja PB, Sethuraman MG (2008) Natural products as corrosion inhibitor for metals in corrosive media - a review. *Mater Lett*. <https://doi.org/10.1016/j.matlet.2007.04.079>
- Raja PB et al (2013) Evaluation of green corrosion inhibition by alkaloid extracts of *Ochrosia oppositifolia* and *Isoreserpiline* against mild steel in 1 M HCl medium. *Ind Eng Chem Res* 52(31):10582–10593
- Ramezanzadeh M, Bahlakeh G, Sanaei Z, Ramezanzadeh B (2018) *Applied Surface Science* Corrosion inhibition of mild steel in 1 M HCl solution by ethanolic extract of eco-friendly *Mangifera indica* (mango) leaves: electrochemical, molecular dynamics, Monte Carlo and ab initio study
- Rani BEA, Basu BBJ (2012) Green inhibitors for corrosion protection of metals and alloys: an overview. *International Journal of Corrosion*. <https://doi.org/10.1155/2012/380217>
- Saini N et al (2019) PVP Oxime-TiO₂-adenine as a hybrid material: decent synthesis and depiction with advanced theoretical measurements for anticorrosive behavior and antibacterial potentiality. *J Mol Liq* 278:438–451. <https://doi.org/10.1016/j.molliq.2019.01.054>
- Sambyal P et al (2018) Progress in organic coatings enhanced anticorrosive properties of tailored poly (aniline-anisidine)/ chitosan / SiO₂ composite for protection of mild steel in aggressive marine conditions. *Prog Org Coat* 119(January):203–213
- Sanaei Z, Ramezanzadeh M, Bahlakeh G (2019) *Journal of Industrial and Engineering Chemistry* Use of *Rosa canina* fruit extract as a green corrosion inhibitor for mild steel in 1 M HCl solution: a complementary experimental, molecular dynamics and quantum mechanics investigation. *J Ind Eng Chem* 69:18–31
- Satapathy AK et al (2009) Corrosion inhibition by *Justicia gendarussa* plant extract in hydrochloric acid solution. *Corros Sci* 51(12):2848–2856
- Shehata OS, Korshed LA, Attia A (2018) Green corrosion inhibitors, past, present, and future. *Corrosion Inhibitors, Principles and Recent Applications*
- Titi A, Mechbal N, El Guerraf A, El Azzouzi M, Touzani R, Hammouti B, Chung I, Lgaz H (2018) Experimental and theoretical studies on inhibition of carbon steel corrosion experimental and theoretical studies on inhibition of carbon steel corrosion by 1, 5 - diaminonaphthalene. *Journal of Bio- and Tribo-Corrosion*. <https://doi.org/10.1007/s40735-018-0140-5>
- Umoren SA, Eduok UM, Solomon MM, Udoh AP (2016) Corrosion inhibition by leaves and stem extracts of *Sida acuta* for mild steel in 1 M H₂SO₄ solutions investigated by chemical and spectroscopic techniques. *Arab J Chem* 9:S209–S224. <https://doi.org/10.1016/j.arabjc.2011.03.008>
- Vijikumar S, Ramanathan K, Devi BP (2011) *Cuscuta reflexa* ROXB . – A Wonderful Miracle Plant in Ethnomedicine. *Indian J Nat Sci* 1(9):676–683.
- Yao W et al (2020) Superhydrophobic coatings for corrosion protection of magnesium alloys. *J Mater Sci Technol* 52:100–118

Publisher's note Springer Nature remains neutral with regard to jurisdictional claims in published maps and institutional affiliations.

Springer Nature or its licensor (e.g. a society or other partner) holds exclusive rights to this article under a publishing agreement with the author(s) or other rightsholder(s); author self-archiving of the accepted manuscript version of this article is solely governed by the terms of such publishing agreement and applicable law.